

Exploiting Digital Surface Models for Inferring Super-Resolution for Remotely Sensed Images

Savvas Karatsiolis, Chirag Padubidri and Andreas Kamilaris

Abstract—Despite the plethora of successful Super-Resolution Reconstruction (SRR) models applied to natural images, their application to remote sensing imagery tends to produce poor results. Remote sensing imagery is often more complicated than natural images and has its peculiarities such as being of lower resolution, it contains noise, and often depicting large textured surfaces. As a result, applying non-specialized SRR models on remote sensing imagery results in artifacts and poor reconstructions. To address these problems, this paper proposes an architecture inspired by previous research work, introducing a novel approach for forcing an SRR model to output realistic remote sensing images: instead of relying on feature-space similarities as a perceptual loss, the model considers pixel-level information inferred from the normalized Digital Surface Model (nDSM) of the image. This strategy allows the application of better-informed updates during the training of the model which sources from a task (elevation map inference) that is closely related to remote sensing. Nonetheless, the nDSM auxiliary information is not required during production and thus the model infers a super-resolution image without any additional data besides its low-resolution pairs. We assess our model on two remotely sensed datasets of different spatial resolutions that also contain the DSM pairs of the images: the DFC2018 dataset and the dataset containing the national Lidar fly-by of Luxembourg. Based on visual inspection, the inferred super-resolution images exhibit particularly superior quality. In particular, the results for the high-resolution DFC2018 dataset are realistic and almost indistinguishable from the ground truth images.

Index Terms—super-resolution reconstruction, remote sensing, nDSM, perceptual loss, deep learning.

I. INTRODUCTION

High-quality aerial photography and satellite imagery facilitate the development of interesting remote sensing applications for large-scale monitoring and earth observation, including land monitoring, urban planning, and surveillance. However, the severe weakness of remotely sensed imagery, in general, is its low spatial resolution. This is due to the cost and time required to collect high-quality/low-noise images and the vulnerability of such images to environmental variations during acquisition like atmospheric and light variations. Excessive costs may diminish the advantages of using high-quality imagery in remote sensing applications. A common alternative to address this limitation is the use of low-quality (low spatial resolution/high noise)

images to reconstruct scene information as much as possible and then perform inference based on the information-enriched data. This strategy maintains the lower image acquisition cost and improves the quality of the final output.

Traditional upscaling methods such as nearest-neighbor and bi-cubic interpolation [1] rely on surrounding pixels to add a small amount of information to an image and tend to produce blurry and distorted results mainly because they fail to recover high-frequency information. Inevitably, demanding applications like small-object detection tasks do not generally benefit much from image interpolation by methods that rely on neighboring pixels to add some level of detail to the image. Some early attempts to produce better results than the traditional interpolation methods involved the learning of degradation models [2] and the feature matching of low/high-resolution patches to facilitate the recovery of high-resolution (HR) images [3]–[5]. Slightly more sophisticated methods built sparse representations that comprised of a dictionary used to reconstruct the HR counterpart of a low-resolution (LR) patch [6], [7]. While image upscaling using sparse representations tends to slightly improve the recovery of high-frequency information, it is a very computationally intensive technique [7]. The limited performance of these approaches in effectively converting a LR image to its realistic HR counterpart originates from them lacking the ability to learn.

One of the reasons that Deep Learning (DL) and Convolutional Neural Networks (CNNs) have become extremely popular is their ability to supply end-to-end models that perform inference based on raw data without relying on hand-engineered features or extensive incorporation of task-related knowledge into the model. These characteristics positioned DL as the mainstream approach nowadays to solving challenging remote sensing tasks. As such, DL is widely used for tackling the Super-Resolution Reconstruction (SRR) task i.e., converting a single LR image to an HR one. The output of the SRR task is called a Super Resolution (SR) image and its goal is to learn how to produce SR images from LR images that are indistinguishable from the ground truth i.e., the HR images. Furthermore, the development of efficient SSR models will greatly benefit DL models performing a plethora of remote sensing tasks since high-quality imagery is especially beneficial for DL models [8]–[11]. With the ever-increasing usage of DL

Corresponding author: Savvas Karatsiolis.

Savvas Karatsiolis is with the CYENS Center of Excellence, Nicosia, Cyprus (e-mail: s.karatsiolis@cyens.org.cy).

Chirag Padubidri is with the CYENS Center of Excellence, Nicosia, Cyprus (e-mail: c.padubidri@cyens.org.cy).

Andreas Kamilaris is with the department of Computer Science, University of Twente, Enschede, The Netherlands (e-mail: a.kamilaris@utwente.nl) and CYENS Center of Excellence, Nicosia, Cyprus (email: a.kamilaris@cyens.org.cy)

methodologies for developing remote sensing applications [12]–[16], training and inferring on HR images greatly increases the chances of obtaining good results on traditionally and notoriously difficult tasks.

II. RELATED WORK

The first attempts of using DL for the SRR task used pixel loss between the SR output and the HR image (ground-truth). Pixel losses are straightforward to implement. Specifically, minimizing the mean squared error (MSE) conveniently maximizes the peak-signal-to-noise ratio (PSNR), which is a commonly used measure for evaluating SRR models. However, PSNR is not a good measure of perceptual similarity because it fails to capture perceptually relevant differences [17]. In particular, the textual detail level is not reflected in the magnitude of the measured PSNR. Pixel losses tend to produce overly smoothed outputs that constitute candidate HR reconstructions: the model calculates a statistical average of the plausible HR reconstructions introduced to it during training. SRCNN [18] was one of the early attempts that used a DL model trained on a pixel loss for the SRR task. Many following attempts experimented with various advanced architectural features in the DL model to mitigate the effects of pixel losses. Kim et al. [19] applied residual learning [20] into a very deep CNN, Zhang et al. [21] applied deep residual channel attention mechanisms and Lai et al. [22] proposed the Laplacian super-resolution network (LapSRN), which supported high up-sampling factors with the use of residual skip connections. Despite the extensive focus on identifying novel architectural features that improve SRR models, the gap between the quality of the HR images and the SR outputs remained. To overcome the limitations created by applying a pixel loss between the ground-truth and the SR image, Johnson et al. [23] introduced a perceptual loss to measure semantic similarity between the two images. They specifically used a VGG-16 [24] model trained on ImageNet [25] and minimized the Euclidean distance between the features of the HR images and the features of the SR images (i.e., a perceptual loss). They showed that this strategy allowed the model to reconstruct fine details and edges. These results are in line with Mahendran and Vedaldi [26] who also showed that matching the features of higher layers in the pre-trained model preserves the image content and the spatial structure of an image. Johnson et al. [23] trained two SRR models: one that did not use any pixel loss during training and relied solely on the perceptual loss and one that only used a pixel loss. The outputs produced by the two models confirmed that while the perceptual loss is better at reconstructing minute details and producing visually appealing results, the pixel loss gives much fewer artifacts mainly because of its smoothing effect on the pixel values. *This result suggests that both losses are useful for the SRR task.*

Further, Generative adversarial networks (GANs) [27] are highly effective generative models for producing realistic images. The GAN learns a mapping from one manifold to another via an adversarial game between a generator model and a real/generated image discriminator model. GAN's ability to produce sharp images by learning the actual data distribution

[27] suggests that the adversarial loss might be a good fit for the SRR task. Indeed, Ledig et al. [17] proposed a GAN-based model for the super-resolution task (SRGAN), combining three losses: a content loss (MSE pixel loss), a perceptual loss (VGG feature matching like in [23]), and an adversarial loss that encourages the network to favor solutions that reside on the manifold of natural images. Wang et al. [28] proposed some improvements to SRGAN including a) the implementation of Residual-in-Residual Dense blocks (RRDBs), which constitute an extension to densely connected networks [29], b) the use of relativistic adversarial loss [30] which stabilizes the GAN's training and improves its performance and c) the application of the perceptual loss before the activations of the VGG layers. Wang et al. called their improved model Enhanced Super-Resolution GAN (ESRGAN). While the ESRGAN's performance on natural images is quite impressive, it tends to create artifacts in remotely sensed imagery [31]. This may emanate from the complexity and variability of the scenes depicted in remote sensing [31] or from the images' lower spatial resolution and the higher noise they usually exhibit. Furthermore, a huge portion of remotely sensed images often includes textured surfaces, in contrast to the images contained in the ImageNet dataset that have more high-frequency components spread throughout the image area.

These peculiarities of remotely sensed images are better managed by models that are oriented to work with such data. In this direction, Gong et al. [31] proposed the Enlighten-GAN model that uses a self-supervised hierarchical perceptual loss. Liu et al. [32] exploited the salient maps of images to learn additional structure priors and to make the model focus more on the salient objects. Huan et al. [33] proposed a multi-scale residual network with hierarchical feature fusion and multi-scale dilation residual blocks. Courtrai et al. [34] used a cycle-GAN [35] to convert LR images to HR images as well as HR images to LR images, which is a process that seems to help the model learn the mapping between the two domains. Courtrai et al. also integrated a YOLOv3 [36] model into their architecture to conduct small object detection. The integrated object detection model, together with the cycle-GAN, train the generator synergically. Despite small object detection being the model's main aim, the generator produces upscaled images to facilitate the task.

Summing up, previous works on the SRR task for remote sensing imagery focus either on the architecture of the model or on small training procedure differentiations that potentially improve the results to a certain extent. In this paper, the authors exploit the best practices derived from state-of-the-art experimentation up to date, suggesting partly keeping the training principles (content and adversarial losses) of the highly successful ESRGAN while modifying the way the perceptual loss is conceived in the context of super-resolution in general and in remote sensing more specifically. The key idea of the proposed approach lies in the observation that single-image super-resolution is an ill-posed problem in the sense that for any LR image, there exist numerous HR images that could correspond to it [23], [31], [32]. Thus, for any successful model to achieve superior performance, it must derive significant

pixel-level knowledge during the training. Up to date, existing most promising models used a perceptual loss that is based on feature matching, i.e., matching the similarity of two images in feature space [17], [23], [28]. Alternatively, the authors propose the replacement of the perceptual loss with a pixel-level loss which is more appropriate for SRR models operating on remotely sensed images. Specifically, the authors exploit the normalized Digital Surface Model (nDSM), defined as the difference between the Digital Surface Model (DSM) and the Digital Elevation Model (DEM), i.e., $nDSM = DSM - DEM$. The nDSM holds a great amount of pixel-level information that can restrain the model's flexibility in outputting a statistical average of viable solutions: a candidate solution must have the same nDSM as the ground-truth HR image. The main difference between the proposed approach and a feature matching perceptual loss is that the nDSM contains most of the spatial relations within an image while feature space similarities may be misleading: semantically unrelated images can have a similar subset of features. Johnson et al. [23] also note this while discussing which VGG layers (lower-level or higher-level) to choose when constructing the perceptual loss. The results of this paper suggest that the gradients flowing from the nDSM back to the SRR model during training improve the quality of the latter. Some task-specific training techniques have also been applied, which stabilize training and improve the results.

III. USING DSMs TO APPLY SUPER RESOLUTION

As mentioned in related work, the ESRGAN model's performance on upscaling natural images is impressive in part due to the perceptual loss used during training. The perceptual loss of ESRGAN is calculated using a second model pre-trained on a second task relevant to the primary task of interest e.g., a classification task conducted via a VGG model. Regarding the ESRGAN's training, the VGG model used for calculating the perceptual loss was trained on the 1000 classes of the ImageNet dataset. This substantial number of classes, in combination with the millions of images contained in the dataset and the effectiveness of the VGG model, facilitated the training of the SRR task. However, remote sensing imagery differs from the images contained in the ImageNet dataset in several aspects and thus a pre-trained VGG model on the ImageNet dataset might not be the best choice for training an SRR model that takes as input aerial photography or satellite imagery. Even if an ESRGAN-like model is trained on a remote sensing task from scratch, using its learned features for building a perceptual loss, it will most probably not be exposed to hundreds of classes or have access to millions of high-resolution images. Such limitations are quite common when dealing with remote sensing tasks. Furthermore, both large textured surfaces and image variability in remote sensing imagery tend to reduce the effectiveness of feature space similarity metrics. In the following subsections, we describe our decisions with respect to the loss functions used in the proposed SRR model.

A. The nDSM-based loss

The authors address the problems imposed to the SRR task of remote sensing imagery by applying a pixel-level loss based on information that is closely related to the domain, harnessing the nDSM. A nDSM inferring model captures the spatial relations in remotely sensed images to infer the heights of the depicted objects. Interestingly, neural networks (NN) predicting depth from single images also use object interactions, like shadows, to identify objects in the scene [37]. To generate nDSM, we use a model developed in previous work [38] that converts single RGB images to nDSMs and we pre-train it with the data used for the SRR task. The model inferring the nDSMs from RGB images uses a U-Net architecture [39] to compress an image into smaller representations, which the model then decodes to form the elevation map. For a detailed model architecture and details regarding its training, we kindly refer the readers to [38]. Figure 1 shows examples of inferring the elevation map of an aerial image via the nDSM model.

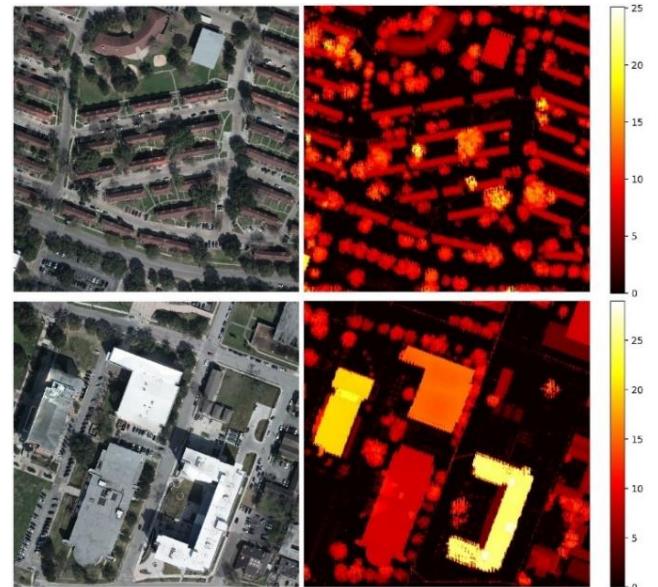


Fig. 1. The nDSM model [38] infers the height map of the objects depicted in an aerial image. The RGB aerial images are shown on the left and the predicted elevation heat maps are shown on the right. The color bars indicate the color-coded height in meters.

The pre-trained nDSM provides the means for defining a loss that closely relates to the domain data. Besides the nDSM-based loss, our proposed SRR methodology also uses a content loss (pixel-loss) and an adversarial loss. The content loss forces the model to output images that maintain the content of the LR image while the adversarial loss drives the model to infer images that are sharper and more realistic.

Ideally, a SR image calculated from its LR counterpart should result in the same nDSM as the ground-truth HR image corresponding to the LR image. The closer an SR image is to the ground-truth HR image, the closer their inferred nDSMs should be. This is reflected in the following loss:

$$L_{nDSM} = \|f_{nDSM}(f_{SR}(x_{LR})) - f_{nDSM}(x_{HR})\|_2 \quad (1)$$

where $f_{nDSM}(x)$ is the output of the nDSM inferring model for input x , $f_{SR}(x)$ is the output of the SRR model for input x and x_{LR} is the LR image. During training, the LR image is used as the input of the SRR model and its SR reconstruction is passed through the pre-trained nDSM model. Then, the ground-truth HR image is also passed through the nDSM model, and the Euclidean distance of the inferred height maps is calculated. *During production, the nDSM model is no longer required*, since its sole purpose is to facilitate the model training by forcing the parameters' update operation to favor weights that output SR images that are similar to the HR images.

B. Adversarial loss

In addition to the content loss and the nDSM loss, we also use an adversarial loss to bias the model toward images that reside on the HR images' manifold. We adopt the original GAN methodology proposed by SRGAN [17] and not the relativistic GAN suggested in ESRGAN [28] because we did not observe any improvements in our results when the latter was used. We noticed however that the proposed nDSM loss stabilizes the training and facilitates learning, which makes the use of a vanilla GAN sufficient. The adversarial loss is defined as

$$L_{adversarial} = \sum_n -\log f_{DGAN}(f_{SR}(x_{LR})) \quad (2)$$

with f_{DGAN} being the discriminator of the GAN, f_{SR} is the SRR model and x_{LR} is the LR image. We use this formulation instead of minimizing $\log(1 - f_{DGAN}(f_{SR}(x_{LR}))$ to avoid the saturating gradient issue [27]. The GAN discriminator is trained on predicting whether input images source from the HR images' distribution or from the SR images' distribution.

C. The proposed super-resolution model architecture

ESRGAN employs the basic architecture of SRGAN [17], incorporating modifications such as the removal of batch normalization [40] everywhere in the model and the use of RRDBs as the basic block of the model. The specific architecture performs most computations in the LR feature space and uses up-scaling units located near the output which increases the resolution of the feature maps calculated by the RRDBs. We apply some further modifications to the ESRGAN architecture that enhance its performance on remote sensing imagery:

- 1) Each sub-pixel up-sampling (x2) layer is followed by two convolutional layers with Parametric Rectified Linear Units (PReLU) [41].
- 2) After the up-sampling units, we use two additional convolutional layers with PReLU activations.
- 3) The output convolutional layer applies a hyperbolic tangent activation function followed by an operation that converts the resulting values in the range [0,1]. Specifically, the rescaling operation applies the function $0.5 \times (x - 1) + 1$ to an input x .

Figure 2 shows the proposed modified architecture for the super-resolution network. The modifications made to the

original ESRGAN architecture are noted in Figure 2. The model implements several blocks, each consisting of three RRDBs that contain residual nodes and dense connections. Each residual node applies a scaling parameter β to the output of each RRDB before adding it to the residual path. A similar scaling is applied at the output of each RRDB and specifically at the residual node that merges the input of the block with its output. Residual scaling prevents instability during the training and allows for smoother updates [28].

D. Content loss

Most SRR models either use Mean Squared Error (MSE) or Mean Absolute Error (MAE) to implement the content loss. While these error functions are a good fit for higher resolution images whose surface depicting portion is not large, this might not be the case for remote sensing imagery.

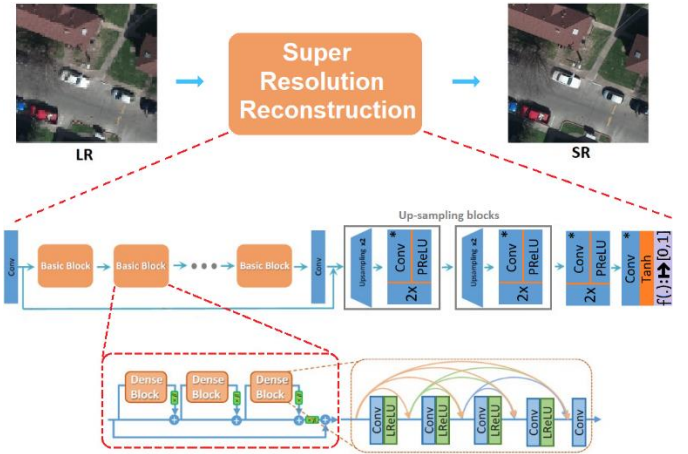


Fig. 2. The modified ESRGAN architecture is used in the proposed super-resolution model. Several RRDBs process the image while maintaining its low-resolution dimensions and upscaling is applied near the output of the model. We introduce two convolutional layers with PReLU activations between the upscaling units as well as two additional convolutional layers with PReLU activations after the last upscaling unit. Furthermore, we use a hyperbolic tangent activation function at the output and a rescaling layer just before the inferred SR image to adjust the values in the range [0,1]. Our modifications on the basic ESRGAN are shown with an asterisk on the right top area of the network components.

As mentioned before, aerial images and (especially) satellite images usually have low resolution and are noisy. Large texture surfaces of wide variety make the SRR task even harder. Images of rocky areas, random soil formations, dumping fields with randomly disposed waste and varied objects' orientation make it extremely hard for a DL model to learn the data distribution. Furthermore, trees with entangled branches and an infinite number of leaves' configurations render the SRR task on remote sensing imagery extremely hard. In particular, soil and leaves' configurations are very complex and thus very hard to model in the super-resolution context. MSE penalizes large prediction errors which makes MAE more suitable when the

dataset contains several outliers. In the case of aerial imagery-based SRR, a wise strategy is to avoid high penalization on the reconstruction error of entities whose distribution is a priori difficult to learn (e.g., soil and trees) and to penalize large errors on easier to learn reconstructions like cars and houses. Thus, we propose the use of the Huber loss [42] over MAE or MSE because it applies either of the two losses, depending on the error magnitude. The content loss expressed as a Huber function with a transition point ϵ and $a = f_{SR}(x_{LR}) - x_{HR}$ is defined as

$$L_{content} = \begin{cases} \frac{1}{2}(a)^2 & \text{if } |a| \leq \epsilon \\ \epsilon(|a|) - \frac{1}{2}\epsilon & \text{otherwise} \end{cases} \quad (3)$$

We propose this design choice after a series of observations made during trial-and-error experimentation with various content losses. Using MAE or MSE, the SRR model tends to predict tree and soil reconstructions with relatively low errors, but reconstructions are overly smooth and blurry. By not heavily penalizing errors of such depictions (trees, soil, or other complicated structures), we shift the burden of generating realistic reconstructions to the other losses (i.e., the nDSM and the adversarial loss). Likewise, by penalizing to a larger degree the reconstruction error of structures like houses and cars, the influence of the nDSM and the adversarial loss is reduced, and the model avoids the generation of high-frequency artifacts. Meyer [43] proposed an alternative probabilistic interpretation of the Huber loss which justifies its use on tasks dealing with aerial photography since these tasks generally contain significant noise and often have low quality: Huber loss minimization relates to minimizing an upper bound on the Kullback-Leibler divergence between the Laplacian distribution of noise in the ground-truth data and the Laplacian distributed prediction noise. Meyer further showed that the optimal transition point of the Huber function is closely related to the noise in the ground-truth data. Taking the above into account, we train the proposed models for minimizing the following combination of the three losses, as described above (content, nDSM, and adversarial loss):

$$L = \alpha L_{nDSM} + L_{content} + \beta L_{adversarial} \quad (4)$$

with α and β being the weighting factors of the losses.

IV. EXPERIMENTS AND RESULTS

We evaluate our methodology with two datasets, one containing images mostly of an urban area taken by an aircraft equipped with image and Ranging Laser Scanner (Lidar) sensors and one dataset containing satellite images mainly of rural areas. Both datasets contain the corresponding DSMs and Digital Elevation Models (DEMs). This variety in landscapes enables us to assess the developed models' performance in different imagery dataset contexts and spatial resolution. As mentioned before, the training of the models requires the nDSM of the area used in the training data while a nDSM is not required during inference. Still, this limitation only allows the use of datasets that include DSMs and DEMs such as the Data Fusion 2018 Contest Dataset (DFC2018) [44], [45] and the dataset containing the national Lidar flyby of Luxembourg,

conducted in 2019 by the country's administration for cadaster and topography [46]-[47]. The DFC2018 dataset is part of a set of community data provided by the IEEE Geoscience and Remote Sensing Society (GRSS). In this paper, we specifically use the Multispectral Lidar Classification Challenge data. The RGB images of the DFC2018 dataset have a $5\text{cm}/\text{pixel}$ spatial resolution and the Lidar resolution is $50\text{cm}/\text{pixel}$. The data belongs to a $4172 \times 1202 \text{ m}^2$ area and includes the University of Houston and its surroundings. The Luxembourg dataset contains RGB images of $20\text{cm}/\text{pixel}$ spatial resolution, and the Lidar resolution is $50\text{cm}/\text{pixel}$. We use the datasets to train two models on the SRR $\times 4$ task (one model for each dataset) and the DFC2018 dataset to train a model on the SRR $\times 8$ task. We do not use the Luxembourg dataset to train a model on the SRR $\times 8$ task because of the poor quality of its downsampled images.

A. Training details

We train our models with the Adam optimizer and a learning rate of 0.0001 , scaling the nDSM and the adversarial losses with factors $\alpha = 0.01$ and $\beta = 0.001$ respectively, as shown in Equation 4. We also apply label smoothing of 0.2 to the GAN training and we pre-train the SRR models with MAE. This puts the weights in an appropriate configuration to avoid local minima and stabilize the GAN training [17]. The MAE of the pre-trained models also provides an indication of what constitutes a suitable value for the transition point of the Huber loss (content loss). Our experiments showed that a Huber loss transition point that is twice the MAE of the pre-trained models gives better results. In our experiments, we use $\times 4$ and $\times 8$ upscale factors. For the $\times 4$ upscale experiments, we train the models with randomly cropped patches of size 520×520 pixels, which are downsampled by means of bicubic interpolation to LR inputs of size 130×130 (the models apply $\times 4$ upscaling and thus the SR outputs match the size of the original HR images). For the $\times 8$ upscale experiment, the 520×520 random patches are downsampled via bicubic interpolation to LR inputs of size 65×65 . The LR images in all experiments are created by downscaling the HR images via bicubic interpolation.

B. Results

Figures 3 and 4 show the results for the SRR $\times 4$ models for the DFC2018 and the Luxembourg datasets respectively. Figure 5 shows the results of the SRR $\times 8$ model for the DFC2018 dataset. The SRR $\times 4$ model dealing with the DFC2018 dataset reconstructs finer image details and more high-frequency components in comparison to the model trained on the Luxembourg dataset. This is not surprising since the resolution of the images in the DFC2018 dataset is four times higher than the resolution of the images in the Luxembourg dataset and thus the model learns the data distribution of a more detailed scenery. This is also reflected in the performance metrics shown in Table I, i.e., the nDSM and SRR models trained with the DFC2018 dataset achieve lower testing errors in terms of the MAE between the inferred output and the ground truth. The SRR model trained with the DFC2018 dataset achieves a higher PSNR and a lower Structural Similarity Index Measure (SSIM)

[48] than the model trained with the Luxembourg dataset for the $SRR \times 4$ task. Table I also shows the values (in parentheses) of PSNR and SSIM achieved via bicubic interpolation of the LR images. The overall findings indicate that the proposed model achieves higher scores for the PSNR and SSIM metrics than in the case where bicubic interpolation is applied. In particular, the increase in the SSIM score is significant.

TABLE I
PERFORMANCE OF THE PROPOSED APPROACH

		DSM (m)	SRR (m)	PSNR (dB)	SSIM
$\times 4$	DFC2018	0.54	0.012	31.17 (28.41)	0.92 (0.83)
	Luxembourg	0.83	0.028	26.46 (24.64)	0.83 (0.68)
$\times 8$	DFC2018	0.54	0.026	28.47 (24.55)	0.886 (0.659)

However, we cannot directly compare the performance of the proposed model with the performance of previous studies on SRR models applied to remote sensing imagery because we could not find reported results on datasets that contain DSMs. On one hand, this is a weakness of this paper, on the other hand, it is a strong point of the paper, as it introduces another dimension in the SRR spectrum of opportunities. Considering this, our assessment relies solely on visual inspection of the results (Figures 3-5) and the significant improvement in the quality metrics' scores (SSIM and PSNR), compared to the basic scenario (bicubic interpolation) (Table I). The results also suggest that the effectiveness of the proposed SRR approach depends on the quality of the nDSM model used. This is one of the reasons why our approach works better on the DFC2018 dataset, as it has a more accurate nDSM. Since the quality of the nDSM model relates to the quality of the images contained in the dataset, the effectiveness of the proposed approach inherently relates to the quality of the images in the dataset. Hence, the results of the $SRR \times 4$ model trained with the high-quality DFC2018 dataset are often indistinguishable from the ground truth HR images.

The proposed SRR models performing $\times 4$ upscaling recover significant information content which was lost during the downscaling of the images (Figures 3-4). Various objects like cars and street poles are properly reconstructed and, in many cases, some fine details like shadows and street lines are almost identical to their HR counterparts. Buildings are also properly reconstructed with high detail levels and large surfaces like rooftops are depicted with their original texture which was severely degraded during downscaling. The reconstructions with the least fidelity are these of trees and soil which is expected given the distribution complexity of their surfaces and their extreme diversity in visual representations. As expected, the results of the SRR model performing $\times 8$ upscaling possess lower fidelity because of the high information loss during the down sampling of the ground truth images. Regardless of the lower quality, the resulting images (Figure 5) recover a lot of details like difficult to identify train rails, rooftop textures, car

shapes, road details, street poles and shadows. The significant image quality improvement observed at the output of the model in comparison to the LR input image reflects the quality metrics' improvement shown in Table I. The results may further justify the use of the proposed model for upscaling LR images to feed other remote sensing models performing challenging tasks that may need an input having a higher level of detail.

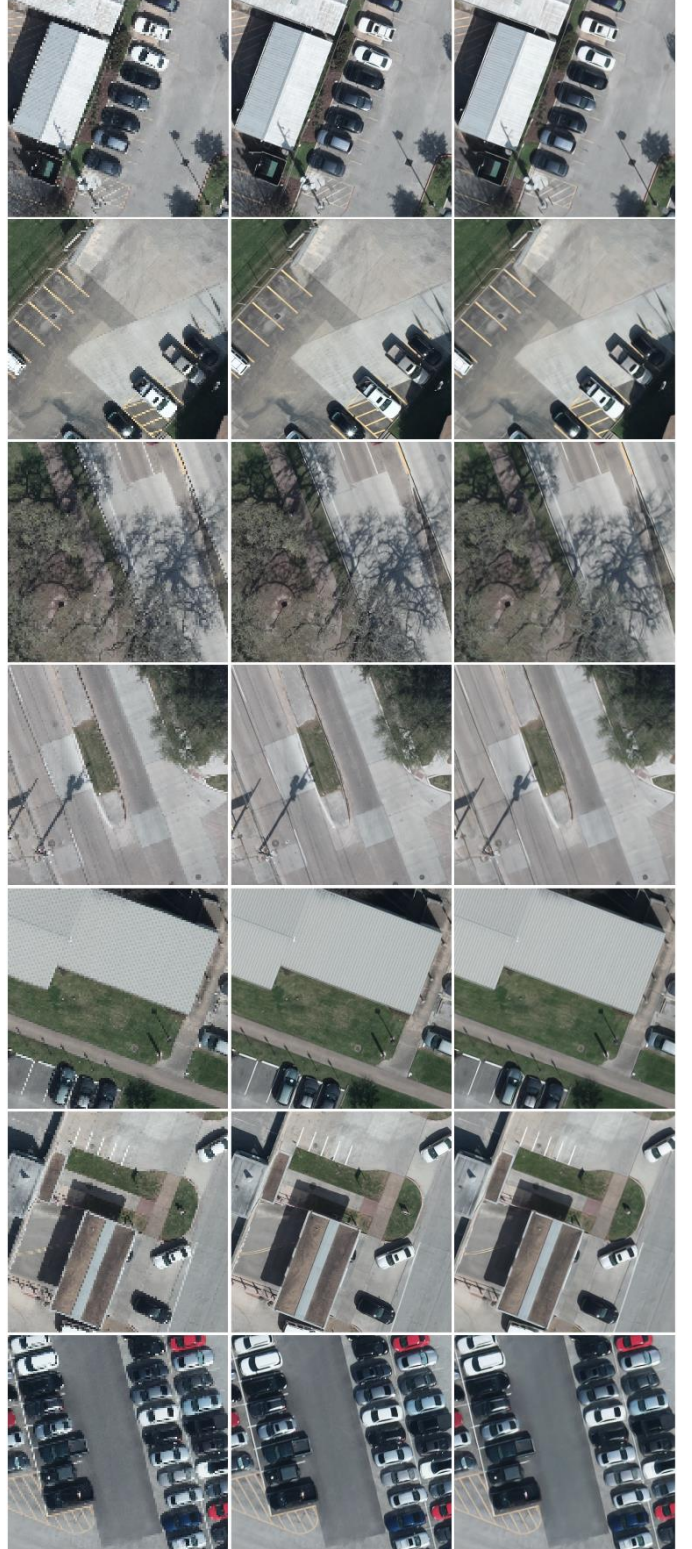




Fig. 3. $SRR \times 4$ results for the DFC2018 dataset. Columns from left to right: LR, HR (ground truth), and SR images (inferred by our model).

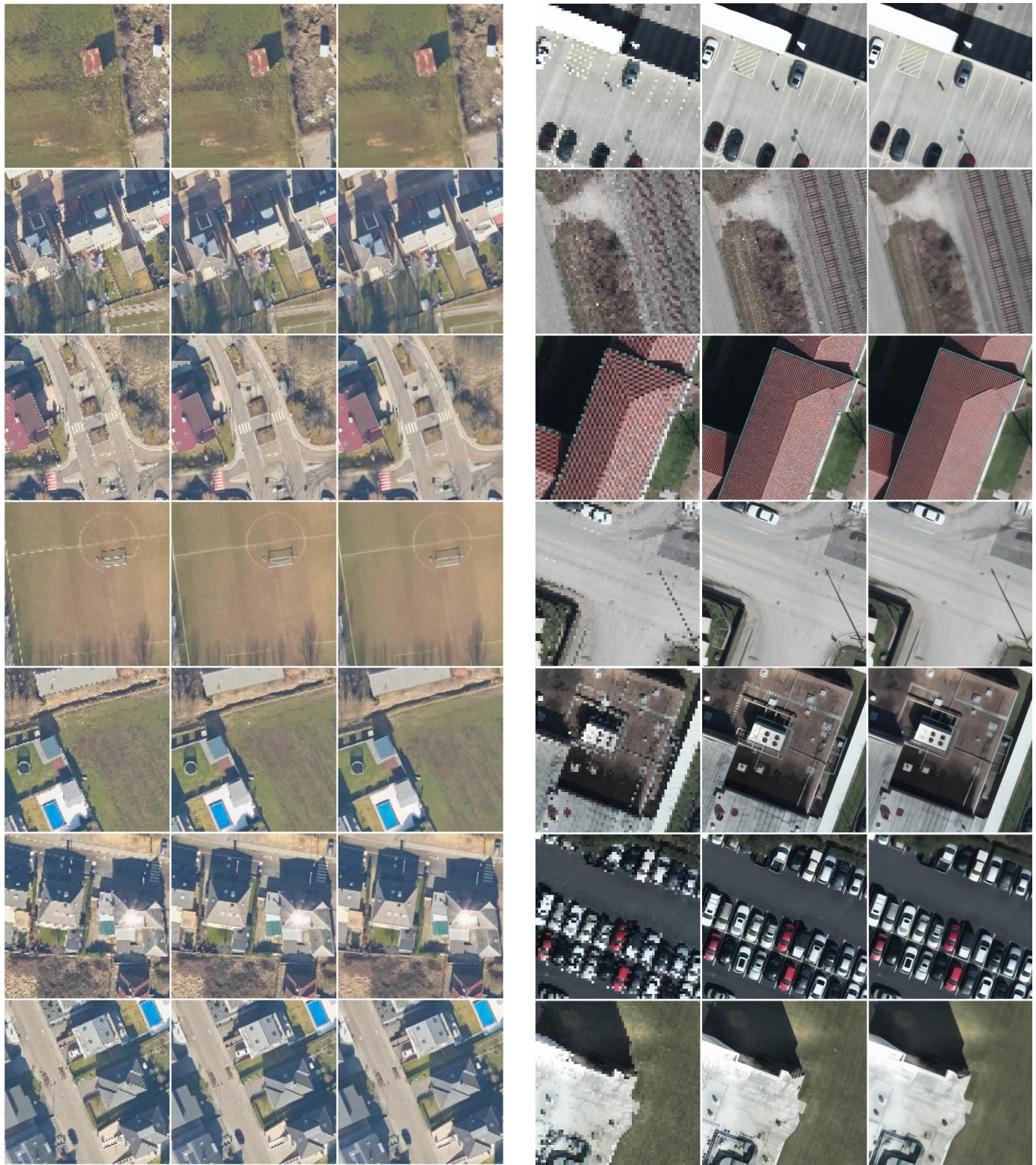


Fig. 4. SRR \times 4 results for the Luxembourg dataset. Columns from left to right: LR, HR (ground truth), and SR images (inferred by our model).

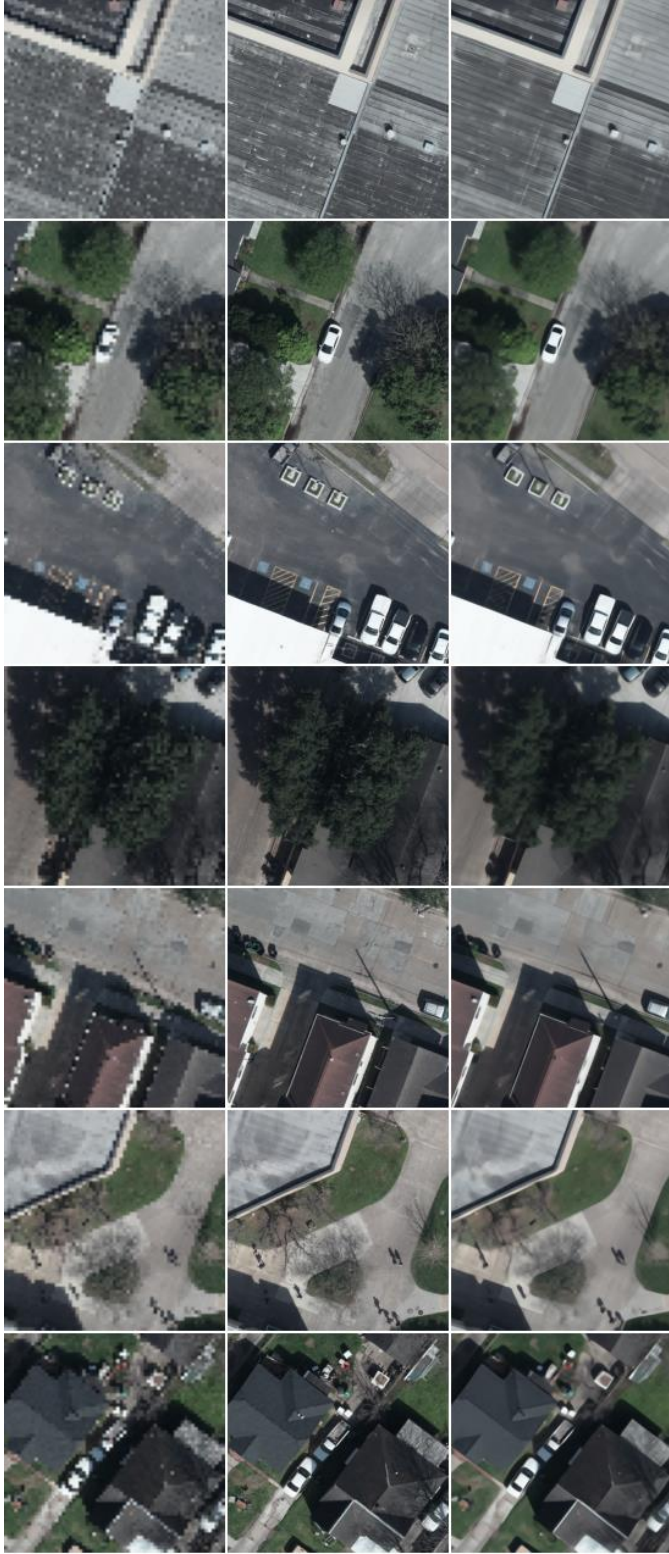


Fig. 5. SRR \times 8 results for the DFC2018 dataset. Columns from left to right: LR, HR (ground truth), and SR images (inferred by our model).

V. CONCLUSION

This paper proposes a super-resolution (SR) reconstruction (SRR) model that works with remotely sensed images, addressing the limitations of existing state-of-the-art models by means of including auxiliary information that is important during the model's training phase, *i.e.*, including the corresponding normalized Digital Surface Model (nDSM) of the remote sensing imagery dataset. In other words, the proposed SRR model, during training, considers the difference between the nDSM inferred by the calculated SR image and the ground truth high resolution (HR) image, instead of using a perceptual loss. Further, the contribution of this paper includes applying some architectural changes to the ESRGAN model and employing a Huber loss as a content loss to mitigate the difficulties imposed by remotely sensed images. Visual inspection, together with the significant improvement of the SSIM and PSNR metrics of the inferred SR images obtained, suggest that the proposed model is suitable for the SRR task and can cope with popular and notorious remote sensing imagery limitations such as big surface textures and lower resolution. Summing up, this paper shows that an nDSM-based loss seems to be suitable for the SRR task on remote sensing imagery, supplying the model with enriched pixel-level information.

REFERENCES

- [1] J. P. Allebach and P. W. Wong, "Edge-directed interpolation," *Proceedings of 3rd IEEE International Conference on Image Processing, Lausanne, Switzerland*, vol. 3, pp. 707–710 vol.3, 1996.
- [2] H. Stark and P. Oskoui, "High-resolution image recovery from image-plane arrays using convex projections," *Journal of the Optical Society of America*, vol. 6, no. 11, pp. 1715–1726, Nov. 1989, doi: 10.1364/JOSAA.6.001715.
- [3] R. Achanta, F. J. Estrada, P. Wils, and S. Süsstrunk, "Salient Region Detection and Segmentation," in *Computer Vision Systems, 6th International Conference, ICVS 2008, Santorini, Greece, May 12-15, 2008, Proceedings*, 2008, vol. 5008, pp. 66–75.
- [4] G. Freedman and R. Fattal, "Image and video upscaling from local self-examples," *ACM Trans. Graph.*, vol. 30, no. 2, pp. 12:1–12:11, 2011, doi: 10.1145/1944846.1944852.
- [5] J. Yang, J. Wright, T. Huang, and Y. Ma, "Image super-resolution as sparse representation of raw image patches," in *2008 IEEE Conference on Computer Vision and Pattern Recognition (CVPR 2008), 24-26 June 2008, Anchorage, Alaska, USA*, 2008, pp. 1–8.
- [6] Y. Zhang, Q. Fan, F. Bao, Y. Liu, and C. Zhang, "Single-Image Super-Resolution Based on Rational Fractal Interpolation," *IEEE Transactions on Image Processing*, vol. 27, no. 8, pp. 3782–3797, 2018, doi: 10.1109/TIP.2018.2826139.
- [7] J. Yang, J. Wright, T. S. Huang, and Y. Ma, "Image Super-Resolution Via Sparse Representation," *IEEE Transactions on Image Processing*, vol. 19, no. 11, pp. 2861–2873, 2010, doi: 10.1109/TIP.2010.2050625.
- [8] V. Thambawita, I. Strümke, S. A. Hicks, P. Halvorsen, S. Parasa, and M. A. Riegler, "Impact of Image Resolution on Deep Learning Performance in Endoscopy Image Classification: An Experimental Study Using a Large Dataset of Endoscopic Images," *Diagnostics, Multidisciplinary Digital Publishing Institute (MDPI)*, vol. 11, no. 12, 2021, doi: 10.3390/diagnostics11122183.
- [9] C. F. Sabotke and B. M. Spieler, "The Effect of Image Resolution on Deep Learning in Radiography," *Radiology: Artificial Intelligence, Radiological Society of North America*, vol. 2, no. 1, p. e190015, 2020.
- [10] M. Koziarski and B. Cyganek, "Impact of Low Resolution on Image Recognition with Deep Neural Networks: An Experimental Study," *International Journal of Applied Mathematics and Computer Science*, vol. 28, no. 4, pp. 735–744, 2018, doi: doi:10.2478/amcs-2018-0056.

[11]S. F. Dodge and L. J. Karam, "Understanding how image quality affects deep neural networks," in *Eighth International Conference on Quality of Multimedia Experience, QoMEX 2016, Lisbon, Portugal, June 6-8, 2016*, 2016, pp. 1–6. doi: 10.1109/QoMEX.2016.7498955.

[12]J. L. Khelifi and M. Mignotte, "Deep Learning for Change Detection in Remote Sensing Images: Comprehensive Review and Meta-Analysis," *IEEE Access*, vol. 8, pp. 126385–126400, 2020, doi: 10.1109/ACCESS.2020.3008036.

[13]Q. Yuan *et al.*, "Deep learning in environmental remote sensing: Achievements and challenges," *Remote Sensing of Environment*, vol. 241, p. 111716, 2020, doi: <https://doi.org/10.1016/j.rse.2020.111716>.

[14]X. Yuan, J. Shi, and L. Gu, "A review of deep learning methods for semantic segmentation of remote sensing imagery," *Expert Systems with Applications*, vol. 169, p. 114417, 2021, doi: 10.1016/j.eswa.2020.114417.

[15]L. P. Osco *et al.*, "A review on deep learning in UAV remote sensing," *International Journal of Applied Earth Observation and Geoinformation*, vol. 102, p. 102456, 2021, doi: <https://doi.org/10.1016/j.jag.2021.102456>.

[16]L. Ma, Y. Liu, X. Zhang, Y. Ye, G. Yin, and B. A. Johnson, "Deep learning in remote sensing applications: A meta-analysis and review," *International Society for Photogrammetry and Remote Sensing (ISPRS)*, vol. 152, pp. 166–177, 2019, doi: <https://doi.org/10.1016/j.isprsjprs.2019.04.015>.

[17]C. Ledig *et al.*, "Photo-Realistic Single Image Super-Resolution Using a Generative Adversarial Network," in *2017 IEEE Conference on Computer Vision and Pattern Recognition, CVPR 2017, Honolulu, HI, USA, July 21-26, 2017*, 2017, pp. 105–114. doi: 10.1109/CVPR.2017.19.

[18]C. Dong, C. C. Loy, K. He, and X. Tang, "Learning a Deep Convolutional Network for Image Super-Resolution," in *European Conference on Computer Vision*, 2014, pp. 184–199.

[19]J. Kim, J. K. Lee, and K. M. Lee, "Accurate Image Super-Resolution Using Very Deep Convolutional Networks," in *IEEE Conference on Computer Vision and Pattern Recognition, CVPR 2016, Las Vegas, NV, USA, June 27-30, 2016*, 2016, pp. 1646–1654. doi: 10.1109/CVPR.2016.182.

[20]K. He, X. Zhang, S. Ren, and J. Sun, "Deep Residual Learning for Image Recognition," in *IEEE Conference on Computer Vision and Pattern Recognition, (CVPR) 2016, Las Vegas, NV, USA, June 27-30, 2016*, 2016, pp. 770–778. doi: 10.1109/CVPR.2016.90.

[21]Y. Zhang, K. Li, K. Li, L. Wang, B. Zhong, and Y. Fu, "Image Super-Resolution Using Very Deep Residual Channel Attention Networks," in *15th European Conference on Computer Vision (ECCV), Munich, Germany, September 8-14, 2018, Proceedings, Part VII*, 2018, vol. 11211, pp. 294–310. doi: 10.1007/978-3-030-01234-2_18.

[22]W.-S. Lai, J.-B. Huang, N. Ahuja, and M.-H. Yang, "Deep Laplacian Pyramid Networks for Fast and Accurate Super-Resolution," in *IEEE Conference on Computer Vision and Pattern Recognition (CVPR) 2017, Honolulu, HI, USA, July 21-26, 2017*, 2017, pp. 5835–5843. doi: 10.1109/CVPR.2017.618.

[23]J. Johnson, A. Alahi, and L. Fei-Fei, "Perceptual Losses for Real-Time Style Transfer and Super-Resolution," in *14th European Conference on Computer Vision (ECCV), Amsterdam, The Netherlands, October 11-14, 2016, Proceedings, Part II*, 2016, vol. 9906, pp. 694–711. doi: 10.1007/978-3-319-46475-6_43.

[24]K. Simonyan and A. Zisserman, "Very Deep Convolutional Networks for Large-Scale Image Recognition," in *3rd International Conference on Learning Representations, ICLR 2015, San Diego, CA, USA, May 7-9, 2015, Conference Track Proceedings*, 2015.

[25]O. Russakovsky *et al.*, "ImageNet Large Scale Visual Recognition Challenge," *International Journal of Computer Vision (IJCV)*, vol. 115, no. 3, pp. 211–252, 2015, doi: 10.1007/s11263-015-0816-y.

[26]A. Mahendran and A. Vedaldi, "Understanding deep image representations by inverting them," in *IEEE Conference on Computer Vision and Pattern Recognition (CVPR), Boston, MA, USA, June 7-12, 2015*, 2015, pp. 5188–5196. doi: 10.1109/CVPR.2015.7299155.

[27]I. J. Goodfellow *et al.*, "Generative Adversarial Nets," in *Proceedings of the 27th International Conference on Neural Information Processing Systems - Volume 2*, 2014, pp. 2672–2680.

[28]X. Wang *et al.*, "ESRGAN: Enhanced Super-Resolution Generative Adversarial Networks," in *European Conference on Computer Vision (ECCV) Workshop, Munich, Germany, September 8-14, 2018, Proceedings, Part V*, 2018, vol. 11133, pp. 63–79. doi: 10.1007/978-3-030-11021-5_5.

[29]G. Huang, Z. Liu, L. van der Maaten, and K. Q. Weinberger, "Densely Connected Convolutional Networks," in *IEEE Conference on Computer Vision and Pattern Recognition (CCVPR), Honolulu, HI, USA, July 21-26, 2017*, 2017, pp. 2261–2269. doi: 10.1109/CVPR.2017.243.

[30]A. Jolicoeur-Martineau, "The relativistic discriminator: a key element missing from standard GAN," 2019.

[31]Y. Gong *et al.*, "Enlighten-GAN for Super-Resolution Reconstruction in Mid-Resolution Remote Sensing Images," *Remote Sensing*, vol. 13, no. 6, 2021, doi: 10.3390/rs13061104.

[32]B. Liu *et al.*, "Saliency-Guided Remote Sensing Image Super-Resolution," *Remote Sensing*, vol. 13, no. 24, 2021, doi: 10.3390/rs13245144.

[33]H. Huan *et al.*, "End-to-End Super-Resolution for Remote-Sensing Images Using an Improved Multi-Scale Residual Network," *Remote Sensing*, vol. 13, no. 4, 2021, doi: 10.3390/rs13040666.

[34]L. Courtrai, M.-T. Pham, and S. Lefèvre, "Small Object Detection in Remote Sensing Images Based on Super-Resolution with Auxiliary Generative Adversarial Networks," *Remote Sensing*, vol. 12, no. 19, 2020, doi: 10.3390/rs12193152.

[35]J.-Y. Zhu, T. Park, P. Isola, and A. A. Efros, "Unpaired Image-to-Image Translation Using Cycle-Consistent Adversarial Networks," in *IEEE International Conference on Computer Vision, ICCV 2017, Venice, Italy, October 22-29, 2017*, 2017, pp. 2242–2251. doi: 10.1109/ICCV.2017.244.

[36]J. Redmon and A. Farhadi, "YOLOv3: An Incremental Improvement," *CoRR*, vol. abs/1804.02767, 2018, [Online]. Available: <http://arxiv.org/abs/1804.02767>

[37]T. van Dijk and G. de Croon, "How Do Neural Networks See Depth in Single Images?", in *IEEE International Conference on Computer Vision, ICCV 2019, Seoul, Korea (South), October 27 - November 2, 2019*, 2019, pp. 2183–2191. doi: 10.1109/ICCV.2019.000227.

[38]S. Karatsiolis, A. Kamilaris, and I. Cole, "IMG2nDSM: Height Estimation from Single Airborne RGB Images with Deep Learning," *Remote Sensing*, vol. 13, no. 12, 2021, doi: 10.3390/rs13122417.

[39]O. Ronneberger, P. Fischer, and T. Brox, "U-Net: Convolutional Networks for Biomedical Image Segmentation," in *18th International Conference on Medical Image Computing and Computer-Assisted Intervention (MICCAI), 2015, Munich, Germany, October 5 - 9, 2015, Proceedings, Part III*, 2015, vol. 9351, pp. 234–241. doi: 10.1007/978-3-319-24574-4_28.

[40]S. Ioffe and C. Szegedy, "Batch Normalization: Accelerating Deep Network Training by Reducing Internal Covariate Shift," in *Proceedings of the 32nd International Conference on Machine Learning (ICML) 2015, Lille, France, 6-11 July 2015*, 2015, vol. 37, pp. 448–456.

[41]K. He, X. Zhang, S. Ren, and J. Sun, "Delving Deep into Rectifiers: Surpassing Human-Level Performance on ImageNet Classification," in *IEEE International Conference on Computer Vision (ICCV) 2015, Santiago, Chile, December 7-13, 2015*, 2015, pp. 1026–1034. doi: 10.1109/ICCV.2015.123.

[42]P. J. Huber, "Robust Estimation of a Location Parameter," *The Annals of Mathematical Statistics*, vol. 35, no. 1, pp. 73 – 101, 1964, doi: 10.1214/aoms/117703732.

[43]G. P. Meyer, "An Alternative Probabilistic Interpretation of the Huber Loss," in *IEEE Conference on Computer Vision and Pattern Recognition (CVPR) 2021, virtual, June 19-25, 2021*, 2021, pp. 5261–5269.

[44]IEEE, "2018 IEEE GRSS Data Fusion Contest." [Online]. Available: <http://dase.grss-ieee.org/index.php> (accessed Feb. 26, 2022).

[45]IEEE, "IEEE France GRSS Chapter." [Online]. Available: <https://site.ieee.org/france-grss/2018/> (accessed Feb. 26, 2022).

[46]Government of the Grand Duchy of Luxembourg, "The Luxembourg data platform, LiDAR 2019 - Digital Surface Model (DSM)." [Online]. Available: <https://data.public.lu/fr/datasets/lidar-2019-modele-numerique-de-la-surface-mns> (accessed Feb. 26, 2022).

[47]Government of the Grand Duchy of Luxembourg, "The Luxembourg data platform, Technical orthophoto of the Grand Duchy of Luxembourg, winter 2019 edition." Accessed: Feb. 26, 2022. [Online]. Available: <https://data.public.lu/fr/datasets/orthophoto-technique-du-grand-duc-de-luxembourg-edition-2019-hiver>

[48]Z. Wang, A. C. Bovik, H. R. Sheikh, and E. P. Simoncelli, "Image quality assessment: from error visibility to structural similarity," *IEEE Transactions on Image Processing*, vol. 13, no. 4, pp. 600–612, 2004, doi: 10.1109/TIP.2003.819861.